Coherent control via weak measurements in ^{31}P single-atom electron and nuclear spin qubits

J. T. Muhonen,[*] J. P. Dehollain,[†] A. Laucht, S. Simmons,[‡] R. Kalra,[§] F. E. Hudson, A. S. Dzurak, and A. Morello[∥]

Centre for Quantum Computation and Communication Technology, School of Electrical Engineering and Telecommunications,
UNSW Sydney, Sydney, New South Wales 2052, Australia

D. N. Jamieson and J. C. McCallum

Centre for Quantum Computation and Communication Technology, School of Physics, University of Melbourne,
Melbourne, Victoria 3010, Australia

K. M. Itoh

School of Fundamental Science and Technology, Keio University, 3-14-1 Hiyoshi, 223-8522, Japan

The understanding of weak measurements and interaction-free measurements has greatly expanded the conceptual and experimental toolbox to explore the quantum world. Here we demonstrate single-shot variable-strength weak measurements of the electron and nuclear spin states of a ^{31}P single-atom donor in silicon. We first show how the partial collapse of the nuclear spin due to measurement can be used to coherently rotate the spin to a desired pure state. We explicitly demonstrate that phase coherence is preserved with high fidelity throughout multiple sequential single-shot weak measurements and that the partial state collapse can be reversed. Second, we use the relation between measurement strength and perturbation of the nuclear state as a physical meter to extract the tunnel rates between the ^{31}P donor and a nearby electron reservoir from data conditioned on observing no tunneling events. Our experiments open avenues to measurement-based state preparation, steering and feedback protocols for spin systems in the solid state, and highlight the fundamental connection between information gain and state modification in quantum mechanics.

I. INTRODUCTION

The quantum measurement postulate, as found in quantum mechanics textbooks, implicitly describes projective (von Neumann) measurements, where a measurement apparatus is coupled to a quantum system and, upon performing the measurement, returns a unique value a_k for some observable $\hat{A}$ of the quantum system. If the system was initially in the state $|\psi\rangle$, the act of measurement leaves it in the state $|\phi_k\rangle$, the eigenstate of the observable $\hat{A}$ with eigenvalue a_k. The nondeterministic and nonunitary process through which the act of measurement transforms the initial state $|\psi\rangle$ into the final state $|\phi_k\rangle$ is known as "wave function collapse" and has been the subject of a century of debate and controversy.

However, as was already appreciated by von Neumann [1], the projective measurement is only a limiting case. One can also have a detector which is only partially correlated with some observable of the quantum system and therefore returns only partial information on the system state. Accordingly, the wave function is not fully projected onto an eigenstate and is only weakly disturbed by the measurement process. The implications and applications of such "weak measurements" and corresponding partial collapse of the quantum state have gained considerable attention, especially in the context of quantum information processing. Recent experiments on superconducting qubits have demonstrated partial wave function collapse [2], measurement reversal [3], stabilized Rabi oscillations using quantum feedback [4], direct observation of quantum trajectories [5,6], reduction of decoherence via "uncollapsing" [7], and observation of the back-action steering from a variable-strength measurement [8,9]. Weak measurements have also been demonstrated with nitrogen-vacancy centers in diamond [10].

Here we describe how to apply the principles of weak quantum measurements to the electron and nuclear spin states of an individual ^{31}P donor atom in silicon. In the context of quantum measurement, the ^{31}P atom provides access to many key features related, e.g., to negative-result measurements [11] and quantum steering [12,13]. In particular, we show that weak single-shot measurements via the electron spin can be used to *phase-coherently* control the state of the ^{31}P nuclear spin and that it is possible to preserve phase coherence with *high fidelity* through *multiple sequential* measurement and control steps. This highlights the potential for measurement-based control in this highly coherent coupled qubit system

———————
[*]Present address: Department of Physics and Nanoscience Center, University of Jyväskylä, P.O. Box 35, 40014 University of Jyväskylä, Finland; juha.t.muhonen@jyu.fi

[†]Present address: QuTech and Kavli Institute of Nanoscience, TU Delft, 2628 CJ Delft, Netherlands.

[‡]Present address: Department of Physics, Simon Fraser University, Burnaby, British Columbia, Canada V5A 1S6.

[§]Present address: School of Mathematics and Physics, University of Queensland, Brisbane, Queensland 4072, Australia.
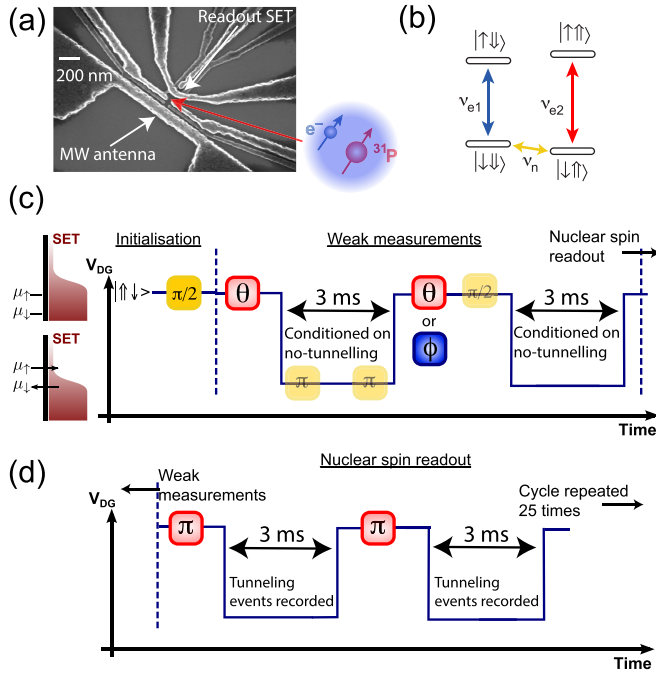
[∥]a.morello@unsw.edu.au

FIG. 1. (a) Scanning electron micrograph of a device identical to the one used in the experiment. A broadband microwave antenna is used to provide both nuclear and electron spin resonance pulses, and a single-electron transistor (SET) detects electron tunneling events in real time. (b) Energy diagram of the electron-nuclear spin system, with labels for the transition frequencies relevant to the present experiments. (c) Pulse sequence for nuclear spin initialization and variable-strength measurement. The solid line represents the combined effect of the voltage of the electrostatic gates V_{DG} adjusting the chemical potential of the donor electron with respect to the SET island, schematically shown on the left. Blue and red boxes represent ESR pulses at ν_{e1} and ν_{e2}, respectively, and yellow boxes represent NMR pulses at ν_n. The semitransparent boxes are needed only for tomography (σ_x and σ_y components). They are, from left to right, two refocusing pulses (around the y axis) and one phase-modulated pulse to define the tomography axis. Timing and pulse lengths are not to scale. Single weak measurements (first column in Fig. 2) require only the first θ pulse and electron readout. (d) Pulse sequence used for nuclear spin readout. An electron readout step initializes the electron spin $|\downarrow\rangle$. An electron spin π pulse is applied at frequency ν_{e2}, which flips the electron spin only if the nuclear spin is $|\Uparrow\rangle$. The nuclear state is assigned $|\Uparrow\rangle$ if a majority of $|\uparrow\rangle$ electrons are detected after 25 repetitions.

and opens avenues to measurement-based state preparation, Einstein-Podolsky-Rosen (EPR) steering, and feedback protocols. We also show how the tunneling rate of the electron to a nearby electron reservoir can be extracted from a data set conditioned on having no tunneling events, in a spirit similar to the Elitzur-Vaidman bomb-testing protocol [14].

II. EXPERIMENT

A. Device

Figure 1(a) shows a scanning electron microscope image of our device, which is fabricated on an isotopically enriched ^{28}Si substrate [15] and where the ^{31}P atom is introduced via

ion implantation [16]. This system contains two natural qubits (the electron spin, with $S = 1/2$ and basis states $|\uparrow\rangle$, $|\downarrow\rangle$, and the ^{31}P nucleus, with spin $I = 1/2$ and basis states $|\Uparrow\rangle$, $|\Downarrow\rangle$) that exhibit extremely long coherence times [17–19] and high quantum gate fidelities [20,21] and can be efficiently entangled with each other [22,23].

The quantum state of the ^{31}P system is accessible through the measurement of the z projection of the electron spin, where z is the axis along which a strong external magnetic field B_0 (≈ 1.5 T in the present experiment) is applied. The donor is placed in close proximity (≈ 20–30 nm [24,25]) to a cold ($T \approx 100$ mK) electron reservoir. Under suitable biasing conditions, the donor-bound electron can tunnel into the cold reservoir if and only if it is in the excited $|\uparrow\rangle$ state. The positively charged donor left behind after this tunneling event shifts the bias point of a nearby single-electron transistor (SET) and switches it to a high-conductance state. The SET current then flows until another electron tunnels into the donor from the reservoir, initializing it again to the ground state. Conversely, a $|\downarrow\rangle$ electron cannot escape the donor, leaving the SET in a near-zero conductance state. This spin-dependent tunneling process [26–28] thus gives rise to a single-shot measurement, with fidelity in excess of 90% [28]. This mechanism provides a near-ideal negative-result measurement for the $|\downarrow\rangle$ state, which is identified by the absence of a signal in the SET current. Importantly, the electron spin is always initialized $|\downarrow\rangle$ after the readout.

The ^{31}P nuclear spin couples to the electron through the hyperfine interaction $A\mathbf{I} \cdot \mathbf{S}$, with $A \approx 97$ MHz in this specific device [19]. As a consequence, the system can have two possible electron spin resonance (ESR) frequencies, $\nu_{e1,2} = \gamma_e B_0 \mp A/2$ [Fig. 1(b)], where $\gamma_e \approx 28$ GHz/T is the electron gyromagnetic ratio. Nuclear readout [Fig. 1(d)] [29] proceeds by initializing the $|\downarrow\rangle$ state and applying a microwave π pulse at, e.g., ν_{e2}, where subsequently measuring the electron $|\uparrow\rangle$ state indicates that the nuclear spin state was $|\Uparrow\rangle$. Since $\gamma_e B_0 \gg A$, the hyperfine interaction can be approximated with $A I_z S_z$. As this commutes with I_z, the readout of the z projection of the nuclear spin is of quantum nondemolition type [30] and can be repeated to achieve a readout fidelity approaching 99.9% [29], well beyond that of a single-shot electron readout. For the (strong) nuclear spin readouts in this paper we perform 25 electron π pulse and readout cycles for each nuclear spin readout.

B. Experimental protocol

The use of an electron π pulse for the nuclear readout is just the limiting case, where one gains maximum information about the nuclear spin state. Here, we explore the more general case where the electron rotation angle is $\theta \neq \pi$, which causes the subsequent electron readout to provide only partial information on the nuclear state. This realizes a novel tunable weak measurement, with strength controlled by the electron rotation angle θ. We show below that, as a result of a weak nuclear measurement conditioned on measuring electron $|\downarrow\rangle$, the nuclear state can be coherently rotated to an arbitrary pure state. This could be extended to provide an interesting implementation of EPR steering [12,13] with spins in the solid state (see Appendix C for more details on EPR steering).

Let us assume that the nuclear spin is initially in the state $|\psi_{n0}\rangle = (|\Downarrow\rangle + |\Uparrow\rangle)/\sqrt{2}$, while the electron spin is initialized in its ground state $|\downarrow\rangle$. We then apply a microwave pulse at frequency ν_{e2} to produce a rotation by an angle θ of the electron spin, conditioned on the nuclear spin being in the $|\Uparrow\rangle$ state. The full electron-nuclear state becomes $|\Psi_{en}\rangle = [|\Downarrow\downarrow\rangle + \cos(\theta/2)|\Uparrow\downarrow\rangle - \sin(\theta/2)|\Uparrow\uparrow\rangle]/\sqrt{2}$. A readout of the electron spin state will produce $|\uparrow\rangle$ with probability $P_\uparrow = \sin^2(\theta/2)/2$ and leave the nuclear spin state $|\Uparrow\rangle$. More interestingly, with probability $P_\downarrow = [1 + \cos^2(\theta/2)]/2$ the electron readout will produce $|\downarrow\rangle$ and leave the nuclear spin in a coherent superposition state $|\psi_n\rangle = [|\Uparrow\rangle + \cos(\theta/2)|\Downarrow\rangle]/\sqrt{1 + \cos^2(\theta/2)}$, which has therefore been *coherently* rotated from the original state $|\psi_{n0}\rangle$ to the pure state

$|\psi_n\rangle$ using only ESR pulses and electron spin measurements. The rotation is probabilistic in the sense that it can fail (if the outcome of the electron readout is $|\uparrow\rangle$), but in the case of a success (heralded by the $|\downarrow\rangle$ electron readout) the end state is fully deterministic.

A more complete description of the process is obtained through a density matrix formalism (for more details, see Appendix A). The initial nuclear spin state is

$$\rho_0 = |\psi_{n0}\rangle\langle\psi_{n0}| = \frac{1}{2}\begin{bmatrix} 1 & 1 \\ 1 & 1 \end{bmatrix}. \qquad (1)$$

After the θ rotation of the electron spin (initially $|\downarrow\rangle$) conditioned on the $|\Uparrow\rangle$ nuclear state and a $|\downarrow\rangle$ electron readout, the nuclear spin is left in the state

$$\rho(\theta) = \frac{1}{1 + \cos^2(\theta/2)}\begin{bmatrix} \cos^2(\theta/2) & \cos(\theta/2) \\ \cos(\theta/2) & 1 \end{bmatrix}, \qquad (2)$$

which notably is a pure state for all values of θ. This readily generalizes to multiple electron rotation and measurement steps. For example, after two sequential applications of the sequence, the nuclear spin state is (conditional on reading $|\downarrow\rangle$ at both steps)

$$\rho(\theta_1, \theta_2) = \frac{1}{1 + \cos^2(\theta_1/2)\cos^2(\theta_2/2)}\begin{bmatrix} \cos^2(\theta_1/2)\cos^2(\theta_2/2) & \cos(\theta_1/2)\cos(\theta_2/2) \\ \cos(\theta_1/2)\cos(\theta_2/2) & 1 \end{bmatrix}, \qquad (3)$$

assuming phase coherence is preserved at the intermediate electron readout step.

An interesting scenario appears if the second electron rotation is applied at ν_{e1} instead of ν_{e2}, so that the rotation is conditioned on the nuclear $|\Downarrow\rangle$ state. Calling ϕ the rotation angle of the microwave pulse at ν_{e1}, the final state becomes

$$\rho(\theta, \phi) = \frac{1}{\cos^2(\phi/2) + \cos^2(\theta/2)}\begin{bmatrix} \cos^2(\theta/2) & \cos(\theta/2)\cos(\phi/2) \\ \cos(\theta/2)\cos(\phi/2) & \cos^2(\phi/2) \end{bmatrix}. \qquad (4)$$

If we set $\phi = \theta$, the final state is $\rho(\theta, \theta) = \rho_0$. This is known as "measurement reversal" [3,31]: the second weak measurement of the nuclear spin erases the effect of the first one.

The nuclear spin rotation by variable-strength measurement is a probabilistic process, conditional on measuring the electron in the $|\downarrow\rangle$ state. The success probability for a single weak measurement step starting from the state in Eq. (1) is $P_1 = [1 + \cos(\theta/2)]/2$. However, since this probability depends on the nuclear spin population at the start of the measurement, the success probability of two sequential weak measurements is not simply this value squared. Rather, the success probability for n sequential weak measurements in our case is $P_n = [1 + \cos(\theta/2)^{2n}]/2$ if all measurements are performed with electron spin rotation θ on the same electron spin resonance frequency.

For the measurement reversal (two weak nuclear measurements, each using a different ESR frequency) the success probability reads $P_{rev} = \cos^2(\theta/2)$, which is notably zero for $\theta = \pi$, as should be expected (one cannot reverse a projective measurement).

III. RESULTS

A. Rotating the nuclear spin state with variable-strength measurements

Figure 2 shows experimental data obtained with full quantum state tomography, i.e., measurement of all three nuclear

spin components $\sigma_z = (\rho_{1,1} - \rho_{2,2})$, $\sigma_x = (\rho_{1,2} + \rho_{2,1})$, and $\sigma_y = i(\rho_{1,2} - \rho_{2,1})$.

The left column of Fig. 2 is the result of a single nuclear rotation step, consisting of an ESR pulse at ν_{e2} rotating the electron spin state around the x axis by angle θ, followed by single-shot electron readout and postselection on the $|\downarrow\rangle$ outcome. Then the nuclear spin is read out with the procedure depicted in Fig. 1(d). The solid lines, in excellent agreement with the data shown in circles, show the expected nuclear state on the basis of the density matrix description presented above without any free fitting parameters. The squares and dashed line show the measured and expected success probability of the protocol.

The middle column in Fig. 2 illustrates the application of two sequential rotation steps, conducted for simplicity with the same ESR rotation angle θ on ν_{e2} at both steps. The fact that the data (especially the σ_x component) follow the theoretical predictions indicates that the nuclear state remains coherent throughout the sequence, which contains two weak nuclear measurements. In other words, the partial collapse of the nuclear state after the first weak measurement is a phase-coherent, predictable process, although the evolution is nonunitary. A minimum requirement for observing this effect is that the dephasing time of the nuclear spin qubit has to be longer than the electron readout time. The ^{31}P nuclear spin qubit in ^{28}Si already has an intrinsically long dephasing time ($T_{2n}^* \approx 0.5$ ms [19] with the donor in the neutral charge
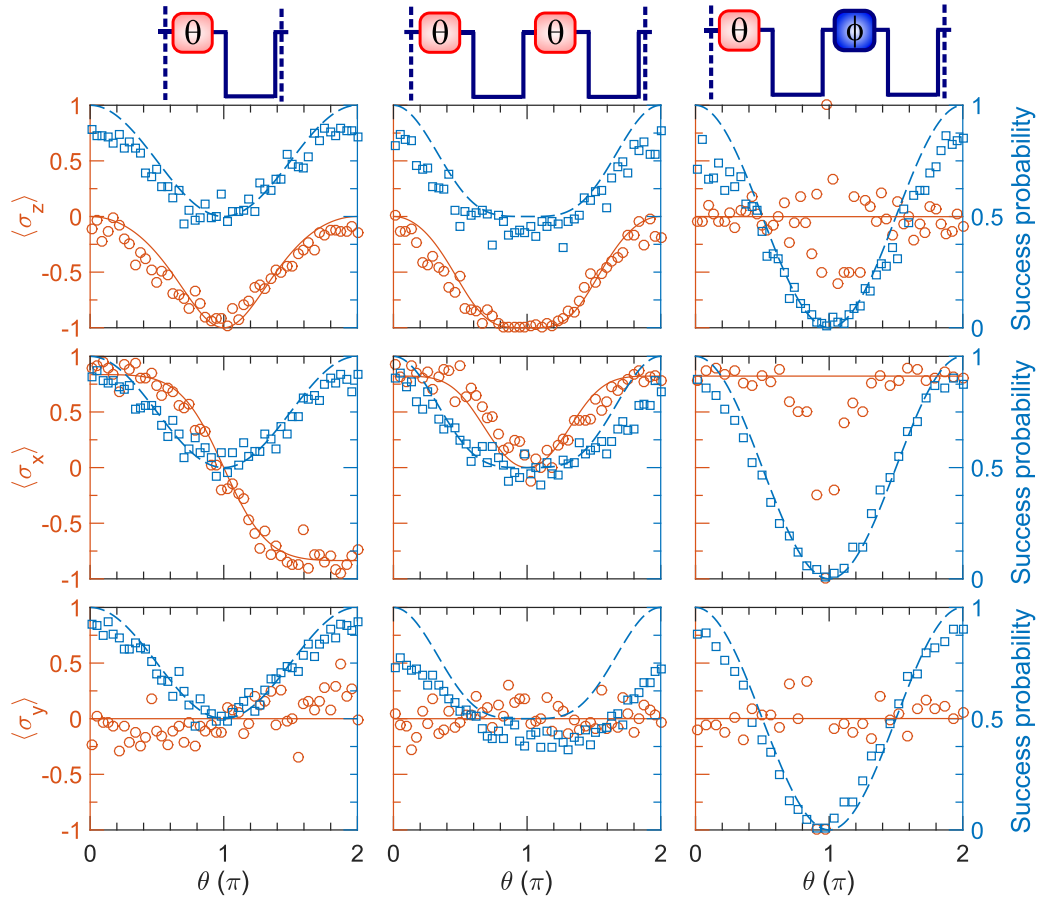
FIG. 2. Quantum control of a nuclear spin with electron spin resonance pulses, observed through quantum state tomography of σ_z (first row), σ_x (second row), and σ_y (third row) as a function of the electron spin rotation angle θ on the ESR frequency ν_{e2}. The columns show, from left to right, one weak measurement, two weak measurements (each with rotation angle θ), and measurement reversal (rotation by θ on ν_{e2} and then by ϕ on ν_{e1}, here $\phi = \theta$). The circles and solid line show the experimental data and theory prediction, respectively, for the expectation value (left axis). The squares and dashed line show the experimental data and theory prediction for the success probability of the protocol. All lines are without any fitting parameters, except the solid lines for σ_x have been scaled by a constant to match the measured asymptotic values. These are not exactly unity presumably due to dephasing-caused rotation errors in the tomography pulse. Each data point corresponds to 200 unconditional repetitions.

state), but here we further extend it by applying two NMR refocusing pulses during the 3-ms electron readout step [see Fig. 1(c)]. We also frequency modulate the NMR source to track the resonance frequency of the nuclear spin qubit during the electron readout phase since the change in the donor electrostatic potential under readout conditions causes a Stark shift of the resonance frequency [25].

A unique feature of our experiment is the high fidelity with which the state prepared by weak measurement overlaps with the target state [as expressed in Eqs. (2) and (3)]. With both single- and double-rotation steps, we measured state fidelities $\mathcal{F} \approx 97\%$, averaged over all rotation angles. We did not observe any significant dependence of the fidelity on the rotation angle [a plot of $\mathcal{F}(\theta)$ is shown in Fig. 4]. These observations suggest that the state fidelity is mainly limited by rotation errors in the tomography pulse.

In the right column of Fig. 2 we present the so-called measurement reversal [3,31], which requires a rotation by θ on ν_{e2} and a rotation by $\phi = \theta$ on ν_{e1}. As predicted, we recover the original state each time (again, conditional on obtaining $|\downarrow\rangle$ at each electron readout step). Note that when $\theta = \pi$,

the nuclear measurement becomes fully projective, and the probability of a successful reversal becomes zero. The data points around $\theta = \pi$ are thus only statistical fluctuations.

B. Using the nuclear spin rotation as a meter for the measurement strength

We now explore the possibility of performing a weak electron spin measurement and the effects that such a measurement has on the nuclear spin. The spin-dependent tunneling mechanism that provides a discrimination between the $|\uparrow\rangle$ and $|\downarrow\rangle$ states yields a fully projective measurement only in the limit $\Gamma_{\uparrow,\text{out}} t_\text{m} \to \infty$, where t_m is the measurement time and $\Gamma_{\uparrow,\text{out}}$ is the tunnel-out rate for a $|\uparrow\rangle$ electron, defined such that the probability for a $|\uparrow\rangle$ electron to have tunneled out of the donor after time t_m is $P_{\uparrow,\text{out}}(t_\text{m}) = 1 - \exp(-\Gamma_{\uparrow,\text{out}} t_\text{m})$. For a finite value of $\Gamma_{\uparrow,\text{out}} t_\text{m}$, the absence of a tunnel-out event constitutes only a weak $|\downarrow\rangle$ measurement.

The effect on the nuclear spin of a weak electron measurement can be captured quantitatively in the density matrix formalism by modifying Eq. (2) to include the probability
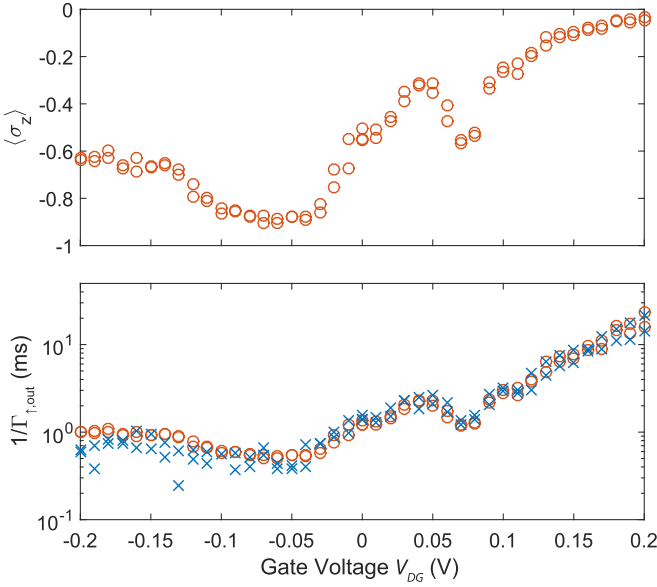
FIG. 3. Extracting electron tunnel rates from a data set conditioned on having no tunneling events. (a) Average nuclear polarization $\langle\sigma_z\rangle$ after a $t_m = 1.5$ ms electron readout window as a function of donor electrochemical potential, controlled by V_{DG}. (b) Electron $|\uparrow\rangle$ tunnel-out time $1/\Gamma_{\uparrow,out}$ extracted from the "tunnel-less" data in (a) using Eq. (8) (circles) and measured directly from tunneling events (crosses). Data are taken by stepping V_{DG} from low to high values and then doing the reverse.

$1 - P_{\uparrow,out}(t_m)$ that a $|\uparrow\rangle$ does not tunnel out within the measurement time:

$$\rho(\theta, t_m)$$
$$= \frac{1}{1 + \cos^2(\theta/2) + [1 - P_{\uparrow,out}(t_m)]\sin^2(\theta/2)}$$
$$\times \begin{bmatrix} \cos^2(\theta/2) + [1 - P_{\uparrow,out}(t_m)]\sin^2(\theta/2) & \cos(\theta/2) \\ \cos(\theta/2) & 1 \end{bmatrix}.$$
(5)

Hence, the expectation value of σ_z as a function of measurement time, conditioned on measuring $|\downarrow\rangle$ (no tunneling), is

$$\langle\sigma_z(t_m)\rangle = \frac{\cos^2(\theta/2) + \exp(-\Gamma_{\uparrow,out}t_m)\sin^2(\theta/2) - 1}{\cos^2(\theta/2) + \exp(-\Gamma_{\uparrow,out}t_m)\sin^2(\theta/2) + 1}, \quad (6)$$

which for $\theta = \pi$ reduces to a particularly simple form,

$$\langle\sigma_z(t_m)\rangle = \frac{\exp(-\Gamma_{\uparrow,out}t_m) - 1}{\exp(-\Gamma_{\uparrow,out}t_m) + 1}. \quad (7)$$

Solving for $\Gamma_{\uparrow,out}$ as a function of $\langle\sigma_z(t_m)\rangle$, we find

$$\frac{1}{\Gamma_{\uparrow,out}} = -\frac{t_m}{\ln\left(\frac{1 + \langle\sigma_z(t_m)\rangle}{1 - \langle\sigma_z(t_m)\rangle}\right)}. \quad (8)$$

Figure 3 shows an experiment where we prepare the nucleus in $|\psi_{n0}\rangle = (|\Downarrow\rangle + |\Uparrow\rangle)/\sqrt{2}$ and the electron in $|\downarrow\rangle$ and then apply an electron π pulse at ν_{e1}, thus leaving the electron-nuclear system in the Bell state [23] $|\Phi^+\rangle = (|\downarrow\Downarrow\rangle + |\uparrow\Uparrow\rangle)/\sqrt{2}$. We then bring the electron towards the readout

position for a time $t_m = 1.5$ ms, and conditional on having no tunneling events, we subsequently measure the nuclear polarization $\langle\sigma_z\rangle$. The experiment is repeated at different values of V_{DG}, which controls the donor electrochemical potential μ_D relative to the Fermi level of the electron reservoir [28] and thereby tunes the donor-reservoir tunnel rate $\Gamma_{\uparrow,out}$. For $V_{DG} \gtrsim 0.2$ V the $|\uparrow\rangle$ state goes below the Fermi level, causing $\Gamma_{\uparrow,out} \approx \Gamma_{\downarrow,out} \approx 0$; that is, the measurement strength vanishes: the absence of a tunneling event does not imply a $|\downarrow\rangle$ state. Accordingly, we find $\langle\sigma_z\rangle \approx 0$ in that limit; that is, the nuclear polarization has not been perturbed from the initial value. For $V_{DG} < 0.2$ V, $1/\Gamma_{\uparrow,out}$ becomes shorter, and $\langle\sigma_z\rangle$ veers towards negative values, which indicates that the electron $|\downarrow\rangle$ measurement is becoming stronger, thus turning the initial $|\Phi^+\rangle$ Bell state towards $|\downarrow\Downarrow\rangle$. Using Eq. (8) we can extract the numerical value of $1/\Gamma_{\uparrow,out}$ and compare it [Fig. 3(b)] to the tunnel time extracted directly from tunneling probabilities. The two methods agree almost perfectly, confirming the validity of our approach. The nonmonotonic behavior of $\Gamma_{\uparrow,out}(V_{DG})$ is related to modulations in the density of states of the electron reservoir [32]. We note that the bandwidth (50 kHz) of the amplifier chain that measures the instantaneous SET current, which depends on the charge state of the donor, is much higher than any of the measured tunnel rates. Therefore, tunnel events that are too fast to be detected are very rare and do not constitute a significant source of errors.

Unlike the weak nuclear measurement described earlier, this process using weak electron measurement does not preserve the purity of the nuclear spin state. Also, the use of a maximally entangled $|\Phi^+\rangle$ Bell state as the starting point of the sequence is inconsequential for this particular experiment; the same result would be obtained starting from an incoherent mixture of $|\downarrow\Downarrow\rangle$ and $|\uparrow\Uparrow\rangle$, although the perfect correlation between the two spins is obviously required. Nonetheless, the process provides a curious example of interaction-free measurement [14] in the solid state.

IV. DISCUSSION

In conclusion, we have shown the application of several concepts and tools of weak single-shot measurements to a model solid-state spin system. We have demonstrated *high-fidelity, coherent* control of the nuclear spin using only ESR pulses and electron spin readout, and we have shown how to measure tunnel rates from data sets without tunneling events. In particular, the high fidelity of the measurement-based control, even after multiple sequential steps, sets ^{31}P spins apart from other qubit systems where single-shot weak measurements have been demonstrated. In the future, these techniques can be applied to a variety of interesting problems, such as the study of qubit dynamics under driving and weak measurement [33], past quantum states of a monitored system [34], and the interplay between measurement and chaotic dynamics [35,36].

APPENDIX A: DENSITY MATRIX CALCULATIONS

Below we refer to the Pauli operators as σ^i, where $i = e, n$ refers to either electron or nuclear spin. We write down the conditional nuclear spin states as they would be after the weak measurement sequence [as presented in Fig. 1(d)] without regard to how the nuclear spin readout is done in practice. One could imagine that this approach might fail for the measurements in Fig. 3, where we use only a short electron readout time and hence the electron state is not initialized to a known state before the strong nuclear spin readout sequence. However, since the full strong nuclear spin readout sequence consists of 25 [electron initialization, ESR pulse, electron readout] cycles, the state of the electron spin at the end of the weak measurement sequence will not significantly affect the final nuclear spin assignment (only the first cycle of the 25 might give an incorrect result).

Given an arbitrary initial state of the nuclear spin described by a density matrix ρ, the effect of the weak nuclear measurement can be described by the conditional rotation matrix

$$U(\theta) = |\Downarrow\rangle\langle\Downarrow| \otimes I + |\Uparrow\rangle\langle\Uparrow| \otimes R(\theta), \tag{A1}$$

$$R(\theta) = \begin{bmatrix} \cos(\theta/2) & -\sin(\theta/2) \\ \sin(\theta/2) & \cos(\theta/2) \end{bmatrix}, \tag{A2}$$

where θ is the rotation angle of the electron spin.

To give a concrete example, we start from the state $\Phi = 1/\sqrt{2}(|\Uparrow\rangle + |\Downarrow\rangle) \otimes |\downarrow\rangle$, i.e., in density matrix form (in the basis $|\Uparrow\uparrow\rangle|\Uparrow\downarrow\rangle|\Downarrow\uparrow\rangle|\Downarrow\downarrow\rangle$)

$$\rho_0 = \frac{1}{2}\begin{bmatrix} 0 & 0 & 0 & 0 \\ 0 & 1 & 0 & 1 \\ 0 & 0 & 0 & 0 \\ 0 & 1 & 0 & 1 \end{bmatrix}. \tag{A3}$$

After the initialization step and the conditional electron spin rotation of angle θ, the state of the system is

$$\rho_\theta = U(\theta)\rho_0 U^\dagger(\theta) = \frac{1}{2}\begin{bmatrix} \sin^2(\theta/2) & -\cos(\theta/2)\sin(\theta/2) & 0 & -\sin(\theta/2) \\ -\cos(\theta/2)\sin(\theta/2) & \cos^2(\theta/2) & 0 & \cos(\theta/2) \\ 0 & 0 & 0 & 0 \\ -\sin(\theta/2) & \cos(\theta/2) & 0 & 1 \end{bmatrix}, \tag{A4}$$

which is an entangled electron-nuclear state for all $\theta \neq 0, 2\pi$ (according to the positive partial transpose (PPT) criterion).

If we then just simply trace out the electron (no conditioning), we obtain the nuclear spin state as

$$\begin{aligned} \rho_n^u &= \mathrm{Tr}_2(\rho_\theta) \\ &= \frac{1}{2}\begin{bmatrix} \sin^2(\theta/2) + \cos^2(\theta/2) & \cos(\theta/2) \\ \cos(\theta/2) & 1 \end{bmatrix} \\ &= \frac{1}{2}\begin{bmatrix} 1 & \cos(\theta/2) \\ \cos(\theta/2) & 1 \end{bmatrix}, \end{aligned} \tag{A5}$$

showing that the expectation value of σ_z^n remains constant independent of θ but the off-diagonal elements decay as a function of the measurement strength. In the limiting case of $\theta = \pi$, we are left with a classical mixture of up and down nuclear spin states.

More interestingly, tracing out the electron conditionally on measuring $|\downarrow\rangle$, we obtain

$$\begin{aligned} \rho_n^c &= \mathrm{Tr}_2[\rho_\theta(I \otimes |\downarrow\rangle\langle\downarrow|)] \\ &= \frac{1}{1 + \cos^2(\theta/2)}\begin{bmatrix} \cos^2(\theta/2) & \cos(\theta/2) \\ \cos(\theta/2) & 1 \end{bmatrix}, \end{aligned} \tag{A6}$$

which is the state in Eq. (2). The second measurement is then simply done by repeating the process starting from the state

$$\rho_\theta^{(2)} = U(\theta)\big(\rho_n^c \otimes |\downarrow\rangle\langle\downarrow|\big)U^\dagger(\theta) \tag{A7}$$

and tracing out similarly. For the measurement reversal we adopt the same procedure but use the rotation matrix for the other electron spin resonance frequency, which reads $U(\theta) = |\Downarrow\rangle\langle\Downarrow| \otimes R(\theta) + |\Uparrow\rangle\langle\Uparrow| \otimes I$. The expectation values for all the nuclear spin components are shown with the data in Fig. 2.

Finally, if we also add a finite electron tunnel-out probability to the process described above, we obtain

$$\begin{aligned} \rho_n^c &= \mathrm{Tr}_2(\rho_\theta\{I \otimes [|\downarrow\rangle\langle\downarrow| + \exp(-\Gamma t)|\uparrow\rangle\langle\uparrow|]\}) \\ &= \frac{1}{1 + \cos^2(\theta/2) + \exp(-\Gamma t)\sin^2(\theta/2)} \\ &\quad \times \begin{bmatrix} \cos^2(\theta/2) + \exp(-\Gamma t)\sin^2(\theta/2) & \cos(\theta/2) \\ \cos(\theta/2) & 1 \end{bmatrix}. \end{aligned} \tag{A8}$$

Note that, unlike all the previous states, this one is not pure unless $\exp(-\Gamma t)\sin^2(\theta/2) = 0$.
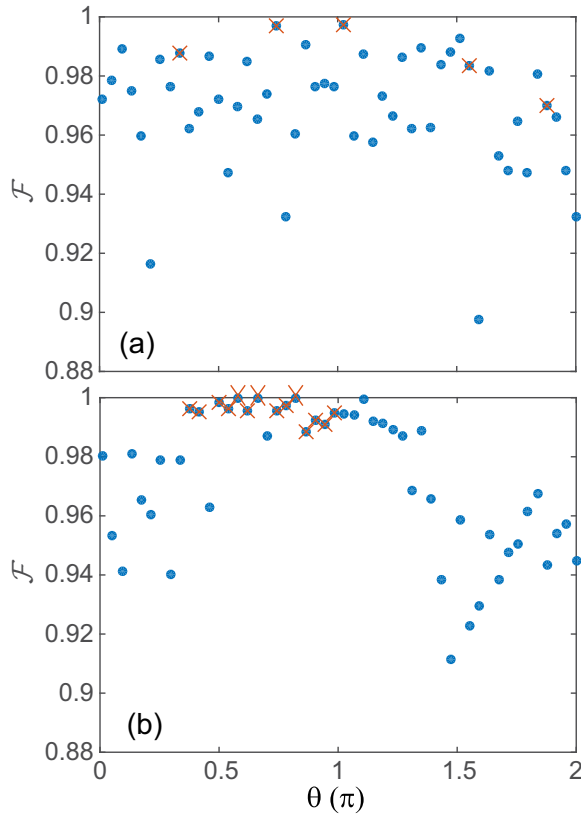
FIG. 4. Final-state fidelity compared to the ideal state as a function of the rotation angle for (a) one or (b) two conditional weak measurements. The average of all points is 0.969(20) in (a) and 0.972(24) in (b). (The value in parentheses indicates the standard deviation of the data points.) The crosses show points where we have forced the state normalization $\sqrt{\langle\sigma_x\rangle^2 + \langle\sigma_y\rangle^2 + \langle\sigma_z\rangle^2} = 1$; see the text.

APPENDIX B: FIDELITY OF NUCLEAR CONTROL BY WEAK MEASUREMENT

Figure 4 shows the fidelity of the nuclear state experimentally prepared using variable-strength measurements compared to the theoretical target state for both the one-measurement and two-measurement cases. We define the state fidelity as $\mathcal{F} = \mathrm{Tr}(\sqrt{\sqrt{\rho_i}\,\rho_m\,\sqrt{\rho_i}})$. The measured density matrix is extracted from the measured expectation values of the spin components $\langle\sigma_{x,y,z}\rangle$ as

$$\rho_m = \frac{1}{2}\begin{bmatrix} 1 + \langle\sigma_z\rangle & \langle\sigma_x\rangle - i\,\langle\sigma_y\rangle \\ \langle\sigma_x\rangle + i\,\langle\sigma_y\rangle & 1 - \langle\sigma_z\rangle \end{bmatrix}. \quad \text{(B1)}$$

The ideal state ρ_i has been defined above and in Eqs. (2) and (3).

Due to the high control and readout fidelity in our system, the measured fidelities are very close to unity. At this level, the finite number of repetitions per point creates statistical fluctuations of a magnitude comparable to the true errors in the state control. As a consequence, we find a few data points where the measured value for $\sqrt{\langle\sigma_x\rangle^2 + \langle\sigma_y\rangle^2 + \langle\sigma_z\rangle^2}$ is actually above unity, meaning that the measured state appears to lie outside the Bloch sphere. This, in turn, can artificially inflate the extracted state fidelity, which relies upon the normaliza-

tion of the density matrices, to the extent that some points produce a nonphysical fidelity above 1. Since this effect would obviously skew the average value of the measurement fidelity by introducing unphysical values, we have chosen to forcibly normalize those states so that $\sqrt{\langle\sigma_x\rangle^2 + \langle\sigma_y\rangle^2 + \langle\sigma_z\rangle^2} = 1$. The normalization factor is applied equally to all three spin components. The points where this normalization was applied are marked with crosses in Fig. 4.

APPENDIX C: NOTES ON EPR STEERING

The use of the word "steering" in the context of quantum systems is somewhat ambiguous in the existing literature. The experiments in this paper demonstrate coherent control of a qubit state by measuring another, correlated qubit state. This is in many contexts called steering, and this usage of the word indeed makes intuitive sense; one is steering the nuclear spin (qubit) by weakly measuring it via the electron (ancilla).

However, it is also common that the word steering, in the quantum context, exclusively refers to what is more exactly known as Einstein-Podolsky-Rosen (EPR) steering. In the operational definition of Wiseman *et al.* [12], EPR steering consists of a "game" where Alice must convince Bob that she has shared with him an entangled state. To do so, she wants to show Bob that she has the ability to control his quantum state by choosing which measurement to perform on her end. This, in turn, can be formalized in experimentally testable EPR steering inequalities.

A demonstration of EPR steering could be conducted on the ^{31}P electron-nuclear system, where "Alice" is the electron spin and "Bob" is the nuclear spin, by following three steps:

(i) Initialize the electron-nuclear system in a maximally entangled Bell state, for example, $|\Phi^+\rangle = (|\downarrow\Downarrow\rangle + |\uparrow\Uparrow\rangle)/\sqrt{2}$, as described in Sec. III B.

(ii) Define different measurement axes for the electron spin. This requires an *unconditional* electron spin rotation, which could be obtained by simultaneously applying ESR pulses of rotation angle θ on both ν_{e1} and ν_{e2}, before a projective electron spin measurement. This is the key
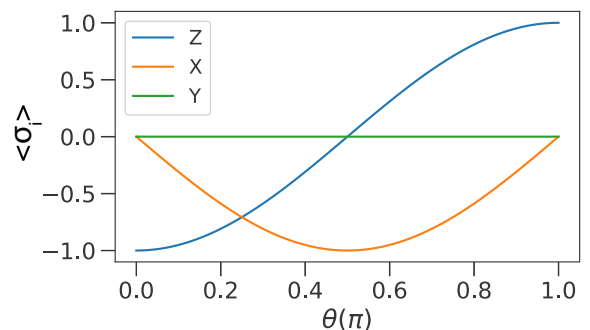

FIG. 5. EPR steering. Theoretical expectation values for the nuclear spin component obtained by starting from the Bell state and performing an *unconditional* rotation of the electron spin with angle θ and then a conditional measurement of the electron. As the unconditional rotation changes the electron measurement basis, one finds a perfect correlation between measuring electron $|\downarrow\rangle$ and nuclear spin Z components at $\theta = 0, \pi$. At $\theta = \pi/2$, there is perfect correlation with the σ_x^n component.

difference between EPR steering and the experiments shown in Sec. III A, where all electron spin rotations were *conditional* on the nuclear spin state (the simultaneous excitation of ν_{e1} and ν_{e2} was not feasible in our experimental setup).

(iii) Conditioned on measuring electron spin $|\downarrow\rangle$, perform nuclear state tomography.

Figure 5 shows the expected nuclear spin components as a function of θ. At $\theta = 0$ the electron spin measurement is along the z axis, and therefore, the subsequent measurement of σ_z^n could be predicted with unity accuracy, whereas the measurement of σ_x^n is completely undetermined. At $\theta = \pi/2$ the electron spin measurement is along the x axis, and now the

reverse is true. This simple simulation captures the essence of EPR steering. The state of Bob's particle tracks exactly the choice of measurement basis made by Alice.

We note that the violation of Bell's inequality has already been demonstrated with the electron-nuclear system studied here [23], and it is known that the requirements for EPR steering are less strict than those for the violation of Bell's inequality. Therefore, using an experimental setup capable of producing two simultaneous microwave pulses at frequencies ν_{e1} and ν_{e2}, it should be possible to demonstrate EPR steering using the ^{31}P system described in the present work.

---

[1] J. von Neumann, *Mathematische Grundlagen der Quantenmechanik* (Springer, Berlin, 1932).

[2] N. Katz, M. Ansmann, R. C. Bialczak, E. Lucero, R. McDermott, M. Neeley, M. Steffen, E. M. Weig, A. N. Cleland, J. M. Martinis, and A. N. Korotkov, Science **312**, 1498 (2006).

[3] N. Katz, M. Neeley, M. Ansmann, R. C. Bialczak, M. Hofheinz, E. Lucero, A. O'Connell, H. Wang, A. N. Cleland, J. M. Martinis, and A. N. Korotkov, Phys. Rev. Lett. **101**, 200401 (2008).

[4] R. Vijay, C. Macklin, D. H. Slichter, S. J. Weber, K. W. Murch, R. Naik, A. N. Korotkov, and I. Siddiqi, Nature (London) **490**, 77 (2012).

[5] K. W. Murch, S. J. Weber, C. Macklin, and I. Siddiqi, Nature (London) **502**, 211 (2013).

[6] S. J. Weber, A. Chantasri, J. Dressel, A. N. Jordan, K. W. Murch, and I. Siddiqi, Nature (London) **511**, 570 (2014).

[7] Y. P. Zhong, Z. L. Wang, J. M. Martinis, A. N. Cleland, A. N. Korotkov, and H. Wang, Nat. Commun. **5**, 3135 (2014).

[8] M. Hatridge, S. Shankar, M. Mirrahimi, F. Schackert, K. Geerlings, T. Brecht, K. M. Sliwa, B. Abdo, L. Frunzio, S. M. Girvin, R. J. Schoelkopf, and M. H. Devoret, Science **339**, 178 (2013).

[9] J. P. Groen, D. Ristè, L. Tornberg, J. Cramer, P. C. de Groot, T. Picot, G. Johansson, and L. DiCarlo, Phys. Rev. Lett. **111**, 090506 (2013).

[10] M. S. Blok, C. Bonato, M. L. Markham, D. J. Twitchen, V. V. Dobrovitski, and R. Hanson, Nat. Phys. **10**, 189 (2014).

[11] R. H. Dicke, Am. J. Phys. **49**, 925 (1981).

[12] H. M. Wiseman, S. J. Jones, and A. C. Doherty, Phys. Rev. Lett. **98**, 140402 (2007).

[13] D. Cavalcanti and P. Skrzypczyk, Rep. Prog. Phys. **80**, 024001 (2017).

[14] A. C. Elitzur and L. Vaidman, Found. Phys. **23**, 987 (1993).

[15] K. M. Itoh and H. Watanabe, MRS Commun. **4**, 143 (2014).

[16] J. van Donkelaar, C. Yang, A. D. C. Alves, J. C. McCallum, C. Hougaard, B. C. Johnson, F. E. Hudson, A. S. Dzurak, A. Morello, D. Spemann, and D. N. Jamieson, J. Phys.: Condens. Matter **27**, 154204 (2015).

[17] A. M. Tyryshkin, S. Tojo, J. J. L. Morton, H. Riemann, N. V. Abrosimov, P. Becker, H.-J. Pohl, T. Schenkel, M. L. W. Thewalt, K. M. Itoh, and S. A. Lyon, Nat. Mater. **11**, 143 (2012).

[18] K. Saeedi, S. Simmons, J. Z. Salvail, P. Dluhy, H. Riemann, N. V. Abrosimov, P. Becker, H.-J. Pohl, J. J. L. Morton, and M. L. W. Thewalt, Science **342**, 830 (2013).

[19] J. T. Muhonen, J. P. Dehollain, A. Laucht, F. E. Hudson, R. Kalra, T. Sekiguchi, K. M. Itoh, D. N. Jamieson, J. C. McCallum, A. S. Dzurak, and A. Morello, Nat. Nanotechnol. **9**, 986 (2014).

[20] J. T. Muhonen, A. Laucht, S. Simmons, J. P. Dehollain, R. Kalra, F. E. Hudson, S. Freer, K. M. Itoh, D. N. Jamieson, J. C. McCallum, A. S. Dzurak, and A. Morello, J. Phys.: Condens. Matter **27**, 154205 (2015).

[21] J. P. Dehollain, J. T. Muhonen, R. Blume-Kohout, K. M. Rudinger, J. K. Gamble, E. Nielsen, A. Laucht, S. Simmons, R. Kalra, A. S. Dzurak, and A. Morello, New J. Phys. **18**, 103018 (2016).

[22] S. Simmons, R. M. Brown, H. Riemann, N. V. Abrosimov, P. Becker, H.-J. Pohl, M. L. Thewalt, K. M. Itoh, and J. J. Morton, Nature (London) **470**, 69 (2011).

[23] J. P. Dehollain, S. Simmons, J. T. Muhonen, R. Kalra, A. Laucht, F. Hudson, K. M. Itoh, D. N. Jamieson, J. C. McCallum, A. S. Dzurak, and A. Morello, Nat. Nanotechnol. **11**, 242 (2016).

[24] F. A. Mohiyaddin, R. Rahman, R. Kalra, G. Klimeck, L. C. Hollenberg, J. J. Pla, A. S. Dzurak, and A. Morello, Nano Lett. **13**, 1903 (2013).

[25] A. Laucht, J. T. Muhonen, F. A. Mohiyaddin, R. Kalra, J. P. Dehollain, S. Freer, F. E. Hudson, M. Veldhorst, R. Rahman, G. Klimeck, K. M. Itoh, D. N. Jamieson, J. C. McCallum, A. S. Dzurak, and A. Morello, Sci. Adv. **1**, e1500022 (2015).

[26] J. M. Elzerman, R. Hanson, L. H. Willems van Beveren, B. Witkamp, L. M. K. Vandersypen, and L. P. Kouwenhoven, Nature (London) **430**, 431 (2004).

[27] A. Morello, C. C. Escott, H. Huebl, L. H. Willems van Beveren, L. C. L. Hollenberg, D. N. Jamieson, A. S. Dzurak, and R. G. Clark, Phys. Rev. B **80**, 081307 (2009).

[28] A. Morello, J. J. Pla, F. A. Zwanenburg, K. W. Chan, K. Y. Tan, H. Huebl, M. Mottonen, C. D. Nugroho, C. Yang, J. A. van Donkelaar, A. D. C. Alves, D. N. Jamieson, C. C. Escott, L. C. L. Hollenberg, R. G. Clark, and A. S. Dzurak, Nature (London) **467**, 687 (2010).

[29] J. J. Pla, K. Y. Tan, J. P. Dehollain, W. H. Lim, J. J. L. Morton, F. A. Zwanenburg, D. N. Jamieson, A. S. Dzurak, and A. Morello, Nature (London) **496**, 334 (2013).

[30] V. B. Braginsky, Y. I. Vorontsov, and K. S. Thorne, Science **209**, 547 (1980).

[31] A. N. Korotkov and A. N. Jordan, Phys. Rev. Lett. **97**, 166805 (2006).

[32] M. Möttönen, K. Y. Tan, K. W. Chan, F. A. Zwanenburg, W. H. Lim, C. C. Escott, J.-M. Pirkkalainen, A. Morello, C. Yang, J. A. van Donkelaar, A. D. C. Alves, D. N. Jamieson, L. C. L. Hollenberg, and A. S. Dzurak, Phys. Rev. B **81**, 161304 (2010).

[33] R. Ruskov, A. Mizel, and A. N. Korotkov, Phys. Rev. B **75**, 220501 (2007).

[34] S. Gammelmark, B. Julsgaard, and K. Mølmer, Phys. Rev. Lett. **111**, 160401 (2013).

[35] J. K. Eastman, J. J. Hope, and A. R. R. Carvalho, Sci. Rep. **7**, 44684 (2017).

[36] V. Mourik, S. Asaad, H. Firgau, J. J. Pla, C. Holmes, G. J. Milburn, J. C. McCallum, and A. Morello, Phys. Rev. E **98**, 042206 (2018).